

**IMECE2008-68021**

## MESOSCOPIC MODEL FOR SIMULATION OF CNT-BASED MATERIALS

**Alexey N. Volkov**

Department of Material Science and Engineering,  
University of Virginia,  
Charlottesville, VA, USA  
av4h@virginia.edu

**Kiril R. Simov**

Department of Material Science and Engineering,  
University of Virginia,  
Charlottesville, VA, USA  
simov@virginia.edu

**Leonid V. Zhigilei**

Department of Material Science and Engineering,  
University of Virginia,  
Charlottesville, VA, USA  
lz2n@virginia.edu

### ABSTRACT

A mesoscopic computational model is developed for simulation of the collective behavior of carbon nanotubes (CNTs) in CNT-based materials. The model adopts a coarse-grained representation of a CNT as a sequence of stretchable cylindrical segments defined by a chain of nodes. The dynamic behavior of CNTs is governed by the equations of motion for the nodes, enabling computationally efficient “molecular dynamics-type” simulations. The internal part of the mesoscopic force field takes into account stretching and bending of individual CNTs. A novel computationally-efficient “tubular” potential method is developed for the description of van der Waals interactions among the nanotubes. The parameterization of the “tubular” potential is based on an interatomic potential for non-bonded interactions between carbon atoms. The application of the mesoscopic model to simulation of systems consisting of hundreds of CNTs demonstrates perfect energy conservation for times as long as tens of nanoseconds. Self-assembly of CNTs into bundles with hexagonal ordering of nanotubes is observed in simulations performed for systems with initial random orientation of CNTs.

### 1. INTRODUCTION

Composite materials based on polymer matrixes reinforced by CNTs is the promising class of materials for electronic, aerospace and other applications [1,2,3]. In these materials, the

unique mechanical, thermal and electronic properties of CNTs are combined with the light weight of polymers. The effective properties of CNT-based nanocomposites depend not only on composition and properties of individual components, but are also strongly affected by the distribution of CNTs in the matrix and the characteristics of the CNT-matrix and CNT-CNT interactions. Theoretical or computational prediction of the effective macroscopic properties of CNT-based nanocomposite materials is a complex problem that has not been resolved yet. Even for systems consisting of CNTs only, such as nanotube mats (bucky paper) [4,5,6], films [7,8,9] and fibers [9], the irregular hierarchical nano/micro-structure of the materials complicates the analysis. In particular, the microscopic structure of bucky paper can be described as a random network of interconnected CNT bundles or ropes [4,5,6], with the rope length as large as hundreds of micrometers [4] and the typical size of pores in this network on the order of hundreds of nanometers [10,11]. Hence, a model suitable for investigation of the properties of CNT-based materials has to include an adequate description of the processes occurring on a broad range of length scales, from the dynamics and interactions of individual CNTs to the collective behavior of a network of CNT bundles with characteristic size on the order of micrometers.

Computationally, properties of individual CNTs have been extensively investigated in atomic-level molecular dynamics simulations, e.g. [1,2,3]. The atomistic modeling, however, is computationally expensive and cannot be used to study dynamic evolution of large ensembles of CNTs at long time

scales. The descriptions based on continuum mechanics [12], e.g. elastic shell or beam models implemented within the framework of the finite element method [13,14,15], are somewhat more efficient than the atomistic models but still not applicable for large-scale dynamic simulations of CNT-based materials. The applications of the elastic shell models have been largely limited to the analysis of the deformation behavior of individual single- and multi-wall CNTs.

Computationally-efficient approach based on the “bead-and-spring” model, commonly used in polymer modeling [16], has been proposed in Ref. [17]. The description of the inter-tube interaction by a spherically-symmetric potential exerted by ‘beads’ on each other, however, coarsens significantly the real nature of inter-tube interactions and can introduce artifacts in the behavior of the model. From the physical point of view, the interaction between the tubes is closer to the interaction between cylindrical segments rather than beads. A mesoscopic representation of CNTs as “breathing flexible cylinders” was introduced in Ref. [18], but the description of the interaction between the tubes was not provided.

In this paper, we extend the mesoscopic representation of CNTs, developed in [18], by adding a description of non-bonding interactions among the nanotubes. A novel computationally-efficient “tubular” potential, explicitly accounting for the cylindrical shape of the interacting CNTs, is developed and implemented in the computational model. The parameterization of the potential is based on an inter-atomic potential used for representation of non-bonding van der Waals interactions between carbon atoms in atomistic simulations. The performance of the model is tested in simulations of self-assembling and bundle formation in a system consisting of hundreds of CNTs.

## 2. DISCRETE MESOSCOPIC MODEL OF CARBON NANOTUBES

A carbon nanotube can be considered as a graphene sheet rolled into a tube in a way ensuring the preservation of periodicity of the hexagonal lattice and capped at the ends by semi-spherical “caps.” The structure and properties of a nanotube with perfect atomic arrangement in the non-deformed state is completely defined by a pair of integers  $(m, n)$  [19], which is often called a CNT type. All the structural parameters of a CNT can be calculated from its type  $(m, n)$ , e.g., the radius of CNT is

$$R_r = l_c \sqrt{3(n^2 + m^2 + nm)} / (2\pi), \quad (1)$$

where  $l_c$  is the carbon-carbon inter-atomic distance in a graphene sheet [19], listed in Table 1.

The typical length,  $L$ , of a CNT in a CNT-based material range from a hundred of nanometers to tens of microns [5,20]. The typical diameter,  $D$ , of tubes obtained, e.g., by HIPCO process or by laser ablation, is on the order of 1 nm [4,6,11].

This means that every tube consists of about  $L \times D / l_c^2 \sim 10^5 \div 10^7$  carbon atoms. This number of atoms is too large for direct atomic-level molecular dynamics simulations of systems consisting of hundreds and thousands of CNTs.

An alternative approach, adapted in this work, is to represent CNTs at a mesoscopic level, by chains of straight cylindrical segments [18]. The length of each segment is chosen to be significantly smaller than the local radius of curvature of the CNT. The interactions among the segment are described by a mesoscopic force field parameterized based on the results of atomistic simulations and/or experimental data. The internal part of the force field including a description of the stretching, bending and torsional deformations of individual CNTs has been given in Ref. [18].

The goal of this paper is to develop a computationally-efficient approach for representation of non-bonding interactions among CNTs. To simplify the initial development and testing of the new “tubular” potential, the model presented in this work includes only the basic features necessary for performing dynamic simulations of a system of interacting CNTs. In particular, the internal part of the force field is represented by the stretching and bending terms only, with radial and torsional degrees of freedom excluded from the model. The initial parameterization of the force field is performed for single-walled CNTs and the effect of the changes in the shapes of local cross-sections of CNTs during the deformation on the strength of non-bonding interactions is neglected.

The general framework of the model, however, is sufficiently flexible to allow for a relatively straightforward extension to modeling of CNTs of different radii, dynamic variation of radii and torsional deformation, description of nanotube buckling and fracture, as well as incorporation of dissipative forces and an approximate representation of the internal energy associated with high-frequency atomic vibrations. These features of the model will be added in the future work as needed for the description of particular aspects of the behavior of CNT-based materials.

Within the assumptions outlined above, the system of interacting CNTs is described in terms of translational motion of nodes located along the axes of the CNTs. The nodes divide CNTs into segments, with each segment defined as a straight section of a CNT between two adjacent nodes.

In a system of  $N$  CNTs, each nanotube  $i$  ( $i = 1, \dots, N$ ) is represented by  $N_i$  nodes (including two end nodes). The state of the nanotube  $i$  can be characterized by the set of position vectors  $\mathbf{r}_{i,j}$  of its nodes,  $\mathbf{R}_i = (\mathbf{r}_{i,1}, \dots, \mathbf{r}_{i,N_i})$ , so that the pair  $(\mathbf{r}_{i,j}, \mathbf{r}_{i,j+1})$  defines the position and orientation of segment  $j$  of the nanotube  $i$ . The dynamics of the system can be described by the equations of motion of classical mechanics in the Lagrangian form [21]

$$\frac{d}{dt} \frac{\partial L}{\partial \dot{\mathbf{R}}} - \frac{\partial L}{\partial \mathbf{R}} = 0, \quad (2)$$

where  $\mathbf{R} = (\mathbf{R}_1, \dots, \mathbf{R}_i, \dots, \mathbf{R}_N)$ ,  $\dot{\mathbf{R}} = d\mathbf{R}/dt$ ,  $L = E(\dot{\mathbf{R}}) - U(\mathbf{R})$  is the Lagrangian of the system,  $E$  and  $U$  are the kinetic and potential energies of the system. In the simplified model considered in this work (see above), the only motion is the translational motion of nanotube nodes and the kinetic energy of the system is

$$E(\dot{\mathbf{R}}) = \sum_{i=1}^N \sum_{j=1}^{N_i} \frac{m_{i,j}}{2} (\dot{\mathbf{r}}_{i,j})^2, \quad (3)$$

where  $m_{i,j}$  is the part of the mass of nanotube  $i$  associated with its node  $j$ . The total potential energy of the system is

$$U(\mathbf{R}) = U_{\text{Str}}(\mathbf{R}) + U_{\text{Bnd}}(\mathbf{R}) + U_{\text{Int}}(\mathbf{R}), \quad (4)$$

where the potential energy of nanotube stretching,  $U_{\text{Str}}(\mathbf{R})$ , bending,  $U_{\text{Bnd}}(\mathbf{R})$ , and inter-tube interaction,  $U_{\text{Int}}(\mathbf{R})$ , can be expressed in the following form:

$$U_{\text{Str}}(\mathbf{R}) = \sum_{i=1}^N \sum_{j=1}^{N_i-1} u_{\text{Str}}(\mathbf{r}_{i,j}, \mathbf{r}_{i,j+1}), \quad (5)$$

$$U_{\text{Bnd}}(\mathbf{R}) = \sum_{i=1}^N \sum_{j=2}^{N_i-1} u_{\text{Bnd}}(\mathbf{r}_{i,j-1}, \mathbf{r}_{i,j}, \mathbf{r}_{i,j+1}), \quad (6)$$

$$U_{\text{Int}}(\mathbf{R}) = \sum_{i=1}^N \sum_{j=i}^N U_{\text{TT}}(\mathbf{R}_i, \mathbf{R}_j). \quad (7)$$

Here,  $u_{\text{Str}}(\mathbf{r}_{i,j}, \mathbf{r}_{i,j+1})$  is the potential energy of stretching of the segment  $(\mathbf{r}_{i,j}, \mathbf{r}_{i,j+1})$ ,  $u_{\text{Bnd}}(\mathbf{r}_{i,j-1}, \mathbf{r}_{i,j}, \mathbf{r}_{i,j+1})$  is the potential energy of the nanotube bending at the node  $\mathbf{r}_{i,j}$ , and  $U_{\text{TT}}(\mathbf{R}_i, \mathbf{R}_j)$  is the potential energy of the interaction between tubes  $i$  and  $j$ . Harmonic potentials parameterized in Ref. [18] based on the results of atomistic simulations are used for the stretching and bending terms of the potential energy, Eqs. (5) and (6).

The development and testing of the potential for calculation of inter-tube interaction energy, Eq. (7), is the main subject of this paper. The ‘‘tubular’’ potential method, designed for evaluation of the CNT-CNT interaction term  $U_{\text{Int}}(\mathbf{R})$ , includes two steps. First, a computationally-efficient ‘‘tubular’’ potential describing interaction between a cylindrical segment and an infinitely-long or semi-infinite straight tube is introduced and described in section 3. Next, using a specially-designed weighed approach, the tubular potential is applied for calculation of interaction between curved tubes. The idea of the weighed approach, substituting the chains of segments participating in the interaction by ‘‘effective’’ straight nanotubes, is described in Section 4. Finally, the new method is tested by performing several simulations of the dynamic structural rearrangements occurring in systems containing hundreds of interacting nanotubes. The analysis of the process of self-organization of CNTs into a random network of close-packed bundles and the corresponding evolution of energy in the system are presented in Section 5.

### 3. TUBULAR POTENTIAL

#### 3.1. Non-bonding Interaction between Carbon Atoms

Following atomic-level computational models, the van der Waals interaction between two CNTs can be described through a sum of pair-wise interactions between all the pairs of carbon atoms that belong to the two CNTs. The non-bonding interaction between two carbon atoms is typically represented by Lennard-Jones interatomic potential [22,23]:

$$\varphi(r) = 4\varepsilon \left[ \left( \frac{\sigma}{r} \right)^{12} - \left( \frac{\sigma}{r} \right)^6 \right], \quad (8)$$

where  $r$  is the distance between the two atoms under consideration. In order to make our model comparable with a popular AIREBO potential, commonly used in atomistic modeling of CNTs and carbon nanostructures, we adopt the functional form and parameters of the potential from Ref. [22]. In particular, the Lennard-Jones potential is modified by a cutoff function  $S(\tau)$  that changes from 1 to 0 when  $r$  is varied from  $r_{c0}$  to  $r_c$  and ensures a smooth transition of the potential to zero at the potential cutoff distance,  $r_c$  [24]. The interatomic potential is then defined as

$$\psi(r) = \varphi(r) S \left( \frac{r - r_{c0}}{r_c - r_{c0}} \right), \quad (9)$$

$$S(\tau) = \Theta(-\tau) + \Theta(\tau)\Theta(1-\tau)[1-\tau^2(3-2\tau)], \quad (10)$$

where  $\Theta(\tau)$  is the Heaviside step function. The values of  $\varepsilon$ ,  $\sigma$ ,  $r_c$ , and  $r_{c0}$  used in the calculations are listed in Table 1, with  $\sigma$  chosen to reproduce the interlayer separation in graphite and  $\varepsilon$  fitted to the elastic constant  $c_{33}$  of graphite.

Parameter	$m_c$ , Da	$l_c$ , Å	$\varepsilon$ , eV	$\sigma$ , Å	$r_c$	$r_{c0}$
Value	12.0107	1.421	0.00284	3.4	$3\sigma$	$2.16\sigma$
Reference		[19]	[22]	[22]	[24]	[24]

**Table 1.** Parameters used as physical input in the design of the mesoscopic ‘‘tubular’’ potential for CNT-CNT interactions: Mass of a carbon atom  $m_c$ , interatomic distance in a graphene sheet  $l_c$ , parameters of Lennard-Jones potential given by Eq. (8), and parameters of the cutoff function in Eq. (9).

#### 3.2. Continuum Tubular Potential for Interaction between a Segment and a Straight Tube

CNT-CNT interaction terms in the right part of Eq. (7) can be reduced to the interactions between pairs of segments:

$$U_{TT}(\mathbf{R}_i, \mathbf{R}_j) = \sum_{k=1}^{N_i-1} \sum_{l=1}^{N_j-1} U_{SS}(\mathbf{r}_{i,k}, \mathbf{r}_{i,k+1}, \mathbf{r}_{j,l}, \mathbf{r}_{j,l+1}), \quad (11)$$

where  $U_{SS}$  is the potential energy of interaction between two corresponding segments. In the case of  $i=j$ , the self-interaction and interaction between neighbor segments is excluded from the summation in Eq. (11). Theoretically,  $U_{SS}$  can be found as a sum of pair potentials, Eq. (9), for all pairs of atoms that belong to the two different segments. In mesoscopic simulations, the number of segments can be as large as millions and every segment consists of many (usually, hundreds or thousands) atoms. Therefore, a direct calculation of the segment-segment potentials  $U_{SS}$  through the summation over atomic pairs is impractical due to obvious limitations of available computer resources.

A more efficient method for calculation of  $U_{SS}$  can be based on a continuum approach, where the summation over interatomic interactions is substituted by the integration over surfaces of the interacting segments. Similar approach was used in Ref. [23] for calculation of the effective potentials describing non-bonding interactions between graphene sheets, fullerene molecules, a fullerene and a straight infinitely-long carbon nanotube, and, in Refs. [23,25], between parallel infinitely-long carbon nanotubes of the same radius. Recently, similar approach was applied for the description of interaction between parallel infinitely-long carbon nanotubes of different radii [26] and used in the derivation of the cohesive law at the CNT/polymer interface [27].

In the continuum approach, the real atomic configurations at surfaces of nanotubes are replaced by the continuous distribution of atoms with surface density  $n_\sigma = 4/(3\sqrt{3}l_c^2)$ ,\* so that the segment-segment potential can be found by integrating the interatomic potential given by Eq. (9) over the surfaces of interacting segments:

$$U_{SS}(h, \alpha, \xi_1, \xi_2, \eta_1, \eta_2) = n_\sigma^2 R_T^2 \int_{\xi_1}^{\xi_2} \int_{\eta_1}^{\eta_2} \int_0^{2\pi} \int_0^{2\pi} \Psi(r(h, \alpha, \xi, \eta, \phi_1, \phi_2)) d\phi_2 d\eta d\phi_1 d\xi \quad (12)$$

Here, the six geometric parameters  $h$ ,  $\alpha$ ,  $\xi_1$ ,  $\xi_2$ ,  $\eta_1$ , and  $\eta_2$ , define the relative position of two segments with respect to each other. In particular,  $h$  and  $\alpha$  are the shortest distance and the angle between the axes of the segments,  $\xi_1$ ,  $\xi_2$  and  $\eta_1$ ,  $\eta_2$  are the coordinates of ends of the first and second segments along their axes with respect to points  $O$  and  $O'$  on the segment axes defining the shortest distance between the axes (see Fig. 1). These geometrical parameters can be found as functions of position vectors of the nodes defining the two segments:  $h = h(\mathbf{r}_1, \mathbf{r}_2, \mathbf{p}_1, \mathbf{p}_2)$ ,  $\alpha = \alpha(\mathbf{r}_1, \mathbf{r}_2, \mathbf{p}_1, \mathbf{p}_2)$ ,  $\xi_1 = \xi_1(\mathbf{r}_1, \mathbf{r}_2, \mathbf{p}_1, \mathbf{p}_2)$ ,  $\xi_2 = \xi_2(\mathbf{r}_1, \mathbf{r}_2, \mathbf{p}_1, \mathbf{p}_2)$ . Integration in Eq. (12) is performed along the axes of the segments,  $\xi$  and  $\eta$ , and over the angles  $\phi_1$  and  $\phi_2$  specifying positions of points in cross-sections of the segments.

Eq. (12) can be used to define the potential for interaction between a segment and an infinitely-long tube by setting the limits of integration,  $\eta_1$  and  $\eta_2$  to infinity:

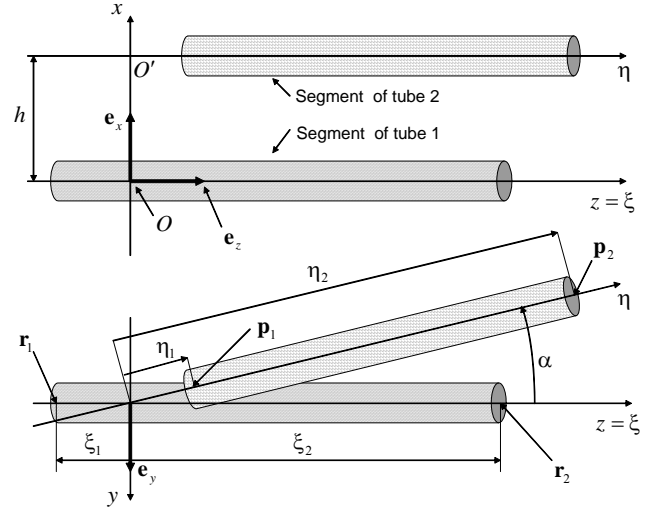


**Figure 1.** Geometric parameters, characterizing the relative position of two cylindrical CNT segments. The axis  $x$  is directed along the shortest distance between the axes of the segments.

$$U_{T\infty}(h, \alpha, \xi_1, \xi_2) = \lim_{\substack{\eta_1 \rightarrow -\infty \\ \eta_2 \rightarrow +\infty}} U_{SS}(h, \alpha, \xi_1, \xi_2, \eta_1, \eta_2) \quad (13)$$

This potential,  $U_{T\infty}$ , defining the interaction between an infinitely long tube and an arbitrary positioned and oriented segment we will call the “tubular” potential. It should be noted, that the continuum approach was applied in Refs. [23,25,26,27] to configurations that are much simpler as compared to the one considered in this work. For example, the continuum potential describing the interaction between a fullerene molecule and an infinitely-long CNT [23] depends on one geometric parameter only. The simplification of the four-dimensional integral in Eq. (13) can be done only for special cases, such as the case of infinitely-long parallel tubes and Lennard-Jones potential without a cutoff [25,26]. In the general case of an arbitrary relative orientation of the tubes, the potential given by Eq. (13) can only be evaluated by numerical integration. This makes calculation of  $U_{T\infty}$  “on the fly,” in the course of a dynamic simulation, impractical. Tabulation of the function of four independent variables with sufficient accuracy is also impossible due to limitations of computer memory. Thus, the design of a computationally-efficient inter-tube potential has to rely on an approximate representation of  $U_{T\infty}$ , which can be expressed through one- or two-dimensional functions only. Such functions could be evaluated and tabulated in advance and used as needed in the course of a dynamics simulation. The design of an approximation of the four-dimensional integral defining the “tubular” potential  $U_{T\infty}$  is presented in the next sub-section.

\* There is a typo in the expression for  $n_\sigma$  in the original version of the paper

### 3.3. Approximate Potential Density and Tubular Potential

The tubular potential  $U_{T\infty}$  can be expressed in terms of the distribution of the potential density  $u_{\infty}(h, \alpha, \xi)$  along the segment axis:

$$U_{T\infty}(h, \alpha, \xi_1, \xi_2) = \int_{\xi_1}^{\xi_2} u_{\infty}(h, \alpha, \xi) d\xi. \quad (14)$$

If the segment and the tube are parallel to each other ( $\alpha = 0$ ), then the potential density for parallel tubes  $u_{\infty\parallel}(h)$  does not depend on  $\xi$  and  $U_{T\infty}(h, \xi_1, \xi_2) = (\xi_2 - \xi_1)u_{\infty\parallel}(h)$ . In this particular case, function  $u_{\infty\parallel}(h)$  can be easily calculated for an arbitrary inter-atomic potential  $\psi(r)$  and recorded in a one-dimensional table with high accuracy. The next step is to find an approximate representation of the potential density for an arbitrary relative orientation of the segment and the tube that can be expressed through one- and two-dimensional functions. The basic idea exploited here is to express the approximate potential density through the potential density for parallel tubes  $u_{\infty\parallel}(h)$ .

Let us consider an infinitesimally thin slice of the segment with coordinate  $\xi$  on the axis  $Oz$ . The thickness of the slice is  $d\xi$  and the surface area is  $dS = 2\pi R_T d\xi$ . The potential  $dU$  of the interaction between the surface of the slice and the infinitely-long tube is equal to  $dU = u_{\infty}(h, \alpha, \xi) d\xi$ . If we rotate the slice around its center so that the axis of the slice becomes parallel to the axes of the tube, then the new slice-tube potential  $d\bar{U} = \bar{u}_{\infty}(h, \alpha, \xi) d\xi$  can be approximately expressed through the potential density for parallel tubes,  $u_{\infty\parallel}$ :

$$\bar{u}_{\infty}(h, \alpha, \xi) = u_{\infty\parallel} \left( \sqrt{h^2 + (\xi \sin \alpha)^2} \right), \quad (15)$$

where  $\sqrt{h^2 + (\xi \sin \alpha)^2}$  is the distance from the center of the slice to the axis of the tube. The comparison of the true  $u_{\infty}(h, \alpha, \xi)$  and approximate  $\bar{u}_{\infty}(h, \alpha, \xi)$  potential densities indicates that the approximation of the true potential density  $u_{\infty}(h, \alpha, \xi)$  by Eq. (15) is only valid for small angles,  $\alpha \leq 10^\circ$ . For larger angles, however, the approximation can be improved by the introduction of two fitting functions,  $\Gamma(h, \alpha)$  and  $\Omega(\alpha)$ , and defining the approximate potential density as follows

$$\tilde{u}_{\infty}(h, \alpha, \xi) = \Gamma(h, \alpha) u_{\infty\parallel} \left( \sqrt{h^2 + (\xi \Omega(\alpha) \sin \alpha)^2} \right). \quad (16)$$

The precision of the approximation (16) depends on the choice of fitting functions, both of which have values on the order of unity. It was found that for CNTs with radius from 3.4 to 15 Å, the fitting functions can be chosen as follows:

$$\Omega(\alpha) = \frac{1}{1 - C_{\Omega} [\Psi_{\Omega}(0) - \Psi_{\Omega}(\alpha)]}, \quad (17)$$

$$\Gamma(h, \alpha) = 1 + [\Gamma_{\perp}(h) - 1] \frac{\Psi_{\Gamma}(\alpha) - \Psi_{\Gamma}(0)}{\Psi_{\Gamma}(\pi/2) - \Psi_{\Gamma}(0)}, \quad (18)$$

$$\Psi_{\Omega}(\alpha) = \exp \left[ -\ln 2 \left( \frac{\alpha - \pi/2}{\alpha_{\Omega}} \right)^2 \right], \quad (19)$$

$$\Psi_{\Gamma}(\alpha) = \exp \left[ -\ln 2 \left( \frac{\alpha - \pi/2}{\alpha_{\Gamma}} \right)^2 \right], \quad (20)$$

where  $C_{\Omega}$ ,  $\alpha_{\Omega}$  and  $\alpha_{\Gamma}$  are constants and the function  $\Gamma_{\perp}(h) = u_{\infty}(h, \pi/2, 0) / u_{\infty\parallel}(h)$  is expressed through the true potential density  $u_{\infty}(h, \alpha, \xi)$  evaluated for the particular case when the tube and the segment are perpendicular to each other ( $\alpha = \pi/2$ ) at point  $\xi = 0$ . It was found that the best choice of  $C_{\Omega}$  depends slightly on the CNTs radius (e.g.,  $C_{\Omega} = 0.23$  for CNTs of type (10,10) and  $C_{\Omega} = 0.25$  for CNTs of type (20,20)), while values  $\alpha_{\Omega} = \pi/4$  and  $\alpha_{\Gamma} = (2/9)\pi$  are appropriate for any CNT from the range of  $R_T$  considered, from 3.4 to 15 Å.

The derivation of Eq. (16) is the key result of this paper. With the help of two tabulated one-dimensional functions,  $u_{\infty\parallel}(h)$  and  $\Gamma_{\perp}(h)$ , this equation allows for a straightforward and computationally efficient calculation of the potential density for an arbitrary relative orientation of a tube and a segment.

Using the approximation given by Eq. (16) in the integral in Eq. (14), the approximate tubular potential can be obtained

$$\begin{aligned} \tilde{U}_{T\infty}(h, \alpha, \xi_1, \xi_2) &= \int_{\xi_1}^{\xi_2} \tilde{u}_{\infty}(h, \alpha, \xi) d\xi = \\ &= \frac{\Gamma(h, \alpha)}{\Omega(\alpha) \sin \alpha} \int_{\xi_1 \Omega(\alpha) \sin \alpha}^{\xi_2 \Omega(\alpha) \sin \alpha} u_{\infty\parallel} \left( \sqrt{h^2 + \bar{\zeta}^2} \right) d\bar{\zeta}. \end{aligned} \quad (21)$$

Introducing a new two-dimensional function  $\Phi(h, \zeta)$

$$\Phi(h, \zeta) = \text{sign}(\zeta) \int_{\zeta_{\min}(h)}^{|\zeta|} u_{\infty\parallel} \left( \sqrt{h^2 + \bar{\zeta}^2} \right) d\bar{\zeta}, \quad (22)$$

one can rewrite Eq. (21) as follows

$$\begin{aligned} \tilde{U}_{T\infty}(h, \alpha, \xi_1, \xi_2) &= \\ &= \frac{\Gamma(h, \alpha)}{\Omega(\alpha) \sin \alpha} [\Phi(h, \xi_2 \Omega(\alpha) \sin \alpha) - \Phi(h, \xi_1 \Omega(\alpha) \sin \alpha)], \end{aligned} \quad (23)$$

where the right part contains two- and one-dimensional functions only. Equations (19), (20) and (23) can be used for  $0 < \alpha < \pi$ , with the values of the approximate tubular potential for other angles calculated based on obvious symmetry considerations. The function  $\zeta_{\min}(h)$  is introduced in the right part of Eq. (22) in order to exclude singularities in sub-integral function physically corresponding to the intersection between nanotube surfaces. If  $h > 2R_T$ , this function is equal to zero.

The true tubular potential given by Eq. (13) is compared with the approximate one of Eq. (23) in Fig. 2. One can see that the choice of the fitting functions in the form of Eqs. (17)–(20) ensures an excellent agreement between the approximate and true potentials.

The approximate potential density for the interaction between a segment and a semi-infinite tube can be introduced

in the form similar to the approximate potential density  $\tilde{u}_\infty$  in Eq. (16). Such a potential density can also be expressed through one- and two-dimensional functions. The potential describing the interaction between a segment and a semi-infinite tube, however, can not be represented in the form similar to Eq. (23). Therefore, this tubular potential is calculated by the numerical integration of the appropriate potential density along the segment axis. Details of the calculation of the tubular potential for a semi-infinite tube will be reported elsewhere [28].

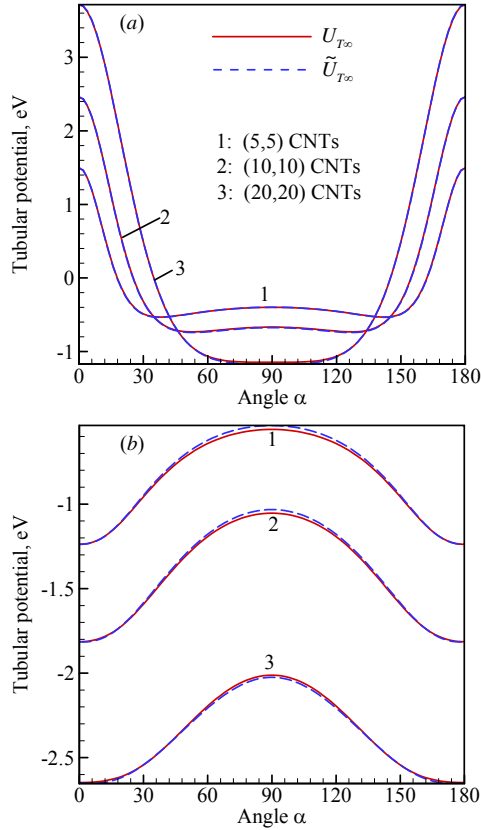


**Figure. 2.** True, Eq. (13), (solid red curves), and approximate, Eq. (23), (dashed blue curves) tubular potentials versus angle  $\alpha$  at  $h-2R_T = r_c/4$  (a) and  $h-2R_T = r_c/3$  (b). In all calculations  $\xi_1 = -10$  Å and  $\xi_2 = 10$  Å. Curves 1–3 are shown for (5,5), (10,10), and (20,20) CNTs, respectively.

For a given radius of CNTs,  $R_T$ , the developed tubular potential, Eq. (23), is completely defined by the interatomic potential,  $\psi(r)$ . In particular, for the cutoff Lennard-Jones potential, Eq. (9), the constants  $C_\Omega$ ,  $\alpha_\Omega$ , and  $\alpha_\Gamma$ , as well as the functions  $u_{x\parallel}(h)$  and  $U_\perp(h)$ , are defined by the parameters listed in Table 1 and the tube radius  $R_T$ . Similarly, the approach for constructing an approximate tubular potential described above can be used for an arbitrary law of interaction between the surface elements representing atoms or molecules that build up the tubular structures. Hence, we believe that, beyond CNTs, the developed potential can be used for the description of the

interaction between various “tubular” nano- and micro objects, such as boron nitride nanotubes, nano- and micro-rods, and bioorganic fibers.

#### 4. WEIGHTED APPROACH FOR CALCULATION OF INTERACTION BETWEEN CURVED NANOTUBES

A special approach should be introduced in order to adopt the tubular potential describing the interaction between a segment and a straight nanotube, Eq. (23), for calculation of inter-tube interaction terms  $U_{TT}$  in Eq. (7) for curved CNTs. In this section, the idea of this approach is demonstrated for a pair of CNTs, where the effects associated with ends of the CNTs are not considered. The general case, when the interactions between the ends of CNTs are included, can be implemented in a similar way and is described elsewhere [28].

##### 4.1. Chains of Interacting Segments

The segment-segment potential  $U_{SS}$  in Eqs. (11) and (12) has a finite range of interaction, i.e.  $U_{SS} = 0$  if the shortest distance  $r_{\min}$  between points at the surfaces of the segments is larger than the cutoff distance of the interatomic potential,  $r_c$ . The summation in Eq. (11), therefore, should include only pairs of segments for which  $r_{\min} < r_c$ . These pairs of segments can be arranged in a “neighbor list,” the approach commonly used to speed up MD simulations [29]. The algorithm for calculation of the shortest distance between the surfaces of two cylindrical bodies, however, is not simple. Instead, one can use a fast approximate approach for building a list of pairs of interacting segments. In this approach the distance between centers of two segments

$$\rho(\mathbf{r}_{i,k}, \mathbf{r}_{i,k+1}, \mathbf{r}_{j,l}, \mathbf{r}_{j,l+1}) = \left| \frac{\mathbf{r}_{j,l} + \mathbf{r}_{j,l+1}}{2} - \frac{\mathbf{r}_{i,k} + \mathbf{r}_{i,k+1}}{2} \right| \quad (24)$$

is compared with the maximum distance above which the two segments can not interact regardless of their orientation with respect to each other:

$$\rho_c(\mathbf{r}_{i,k}, \mathbf{r}_{i,k+1}, \mathbf{r}_{j,l}, \mathbf{r}_{j,l+1}) = \left[ \left( \frac{L_{i,k}}{2} \right)^2 + R_T^2 \right]^{1/2} + \left[ \left( \frac{L_{j,l}}{2} \right)^2 + R_T^2 \right]^{1/2} + r_c, \quad (25)$$

where  $L_{i,k}$  and  $L_{j,l}$  are the lengths of the corresponding segments. Hence, a pair of segments is added to the list of potential neighbors only if the condition

$$\rho(\mathbf{r}_{i,k}, \mathbf{r}_{i,k+1}, \mathbf{r}_{j,l}, \mathbf{r}_{j,l+1}) \leq \rho_c(\mathbf{r}_{i,k}, \mathbf{r}_{i,k+1}, \mathbf{r}_{j,l}, \mathbf{r}_{j,l+1}) \quad (26)$$

is satisfied.

One can re-write Eq. (11) in the form

$$U_{TT}(\mathbf{R}_i, \mathbf{R}_j) = \frac{1}{2} \left[ \sum_{k=1}^{N_i-1} U_{ST}(\mathbf{r}_{i,k}, \mathbf{r}_{i,k+1}, \mathbf{R}_j) + \sum_{k=1}^{N_j-1} U_{ST}(\mathbf{r}_{j,k}, \mathbf{r}_{j,k+1}, \mathbf{R}_i) \right], \quad (27)$$

where  $U_{ST}(\mathbf{r}_{i,k}, \mathbf{r}_{i,k+1}, \mathbf{R}_j)$  is the potential of interaction between segment  $(\mathbf{r}_{i,k}, \mathbf{r}_{i,k+1})$  and the whole tube  $\mathbf{R}_j$ . As soon as all pairs of possibly interacting segments are found, one can identify continuous chains of segments within the tube  $\mathbf{R}_j$  that interact with segment  $(\mathbf{r}_{i,k}, \mathbf{r}_{i,k+1})$ . Correspondingly, the segment-tube potential  $U_{ST}(\mathbf{r}_{i,k}, \mathbf{r}_{i,k+1}, \mathbf{R}_j)$  can be represented in the form

$$U_{ST}(\mathbf{r}_{i,k}, \mathbf{r}_{i,k+1}, \mathbf{R}_j) = \sum_m U_{SC}(\mathbf{r}_{i,k}, \mathbf{r}_{i,k+1}, \mathbf{q}_{1,m}, \dots, \mathbf{q}_{N_m,m}), \quad (28)$$

where  $U_{SC}(\mathbf{r}_{i,k}, \mathbf{r}_{i,k+1}, \mathbf{q}_{1,m}, \dots, \mathbf{q}_{N_m,m})$  is the potential of interaction between a segment  $(\mathbf{r}_{i,k}, \mathbf{r}_{i,k+1})$  in CNT  $\mathbf{R}_i$  and a chain of segments  $(\mathbf{q}_{1,m}, \dots, \mathbf{q}_{N_m,m})$  in CNT  $\mathbf{R}_j$ . The summation over  $m$  accounts for CNT configurations in which more than one separate chain of segments in CNT  $\mathbf{R}_j$  interacts with segment  $(\mathbf{r}_{i,k}, \mathbf{r}_{i,k+1})$ . Such configurations may appear, for example, when CNT  $\mathbf{R}_j$  forms a loop enclosing segment  $(\mathbf{r}_{i,k}, \mathbf{r}_{i,k+1})$ .

#### 4.2. Approximate Weighted Segment-Chain Potential

The maximum length of chains interacting with any segment in Eq. (28) is defined by the length of the CNT segments and the cutoff distance for interatomic interaction. The high stiffness of CNTs ensures that, for appropriate choice of the model parameters, the length of the chains is small compared to a typical radius of curvature of nanotubes. Thus, one can neglect the curvature of the chains and calculate every term in the sum in the right part of Eq. (28), assuming that the corresponding chain is a part of a straight tube.

To simplify the notation, let us consider an interaction of a segment  $(\mathbf{r}_1, \mathbf{r}_2)$  with a chain of segments  $(\mathbf{q}_1, \dots, \mathbf{q}_N)$  in one on the neighboring CNTs. If the chain does not include the tube ends, then the segment-chain interaction can be calculated with the help of the tubular potential given by Eq. (23), i.e.,

$$U_{SC}(\mathbf{r}_1, \mathbf{r}_2, \mathbf{q}_1, \dots, \mathbf{q}_N) = \tilde{U}_{T\infty} \left( h(\mathbf{r}_1, \mathbf{r}_2, \mathbf{p}_1, \mathbf{p}_2), \alpha(\mathbf{r}_1, \mathbf{r}_2, \mathbf{p}_1, \mathbf{p}_2), \xi_1(\mathbf{r}_1, \mathbf{r}_2, \mathbf{p}_1, \mathbf{p}_2), \xi_2(\mathbf{r}_1, \mathbf{r}_2, \mathbf{p}_1, \mathbf{p}_2) \right). \quad (29)$$

Here,  $\mathbf{p}_1$  and  $\mathbf{p}_2$  are position vectors of two points defining an ‘effective’ straight tube representing the chain of segments  $(\mathbf{q}_1, \dots, \mathbf{q}_N)$ . In order to ensure the conservation of energy in a dynamic simulation, functions  $\mathbf{p}_k(\mathbf{r}_1, \mathbf{r}_2, \mathbf{q}_1, \dots, \mathbf{q}_N)$  should be continuous and should have continuous derivatives even at a time when the list of segments in the chain is changing due to the relative motion of CNTs. A possible way to satisfy this condition is to define  $\mathbf{p}_k$  as a weighted average of the positions of nodes in the chain:

$$\mathbf{p}_1 = \frac{1}{W} \sum_{j=1}^{N-1} w_{j+1/2} \mathbf{q}_j, \quad \mathbf{p}_2 = \frac{1}{W} \sum_{j=1}^{N-1} w_{j+1/2} \mathbf{q}_{j+1}, \quad W = \sum_{j=1}^{N-1} w_{j+1/2}, \quad (30)$$

where  $w_{j+1/2} = w(\mathbf{r}_1, \mathbf{r}_2, \mathbf{q}_j, \mathbf{q}_{j+1})$  is a smooth weight function for the pair of segments  $(\mathbf{r}_1, \mathbf{r}_2)$  and  $(\mathbf{q}_j, \mathbf{q}_{j+1})$ . The weight function serves as a measure of relative proximity of these two segments and should approach zero as the distance between the segments reaches the limit of their interaction given by Eq. (25). For example, the weight function can be defined as

$$w(\mathbf{r}_1, \mathbf{r}_2, \mathbf{q}_j, \mathbf{q}_{j+1}) = S \left( \frac{\rho(\mathbf{r}_1, \mathbf{r}_2, \mathbf{q}_j, \mathbf{q}_{j+1}) - \rho_{\min}}{\rho_c(\mathbf{r}_1, \mathbf{r}_2, \mathbf{q}_j, \mathbf{q}_{j+1}) - \rho_{\min}} \right), \quad (31)$$

where  $S(\tau)$  is the universal switching function defined by Eq. (10) and  $\rho_{\min}$  is a constant parameter equal to the distance between centers of segments below which the weight function is assumed to be equal to unity.

Hence, the developed approach for calculation of the inter-tube interaction term in Eq. (7) includes the following four basic steps:

1. Calculation of pairs of neighbor segments with the help of the condition given by Eq. (26).
2. For every segment, its neighbor segments are grouped into chains, constituting continuous sequences of segments belonging to the same nanotube.
3. For every segment-chain pair, the position vectors  $(\mathbf{p}_1, \mathbf{p}_2)$  defining an ‘effective’ straight nanotube are calculated with Eq. (30), and the interaction potential  $U_{SC}$  is calculated using the tubular potential according to Eq. (29).
4. Finally, the total inter-tube interaction energy of all segments is calculated by summing the contributions of all segment-chain pair according to Eqs. (27)–(28).

## 5. COMPUTATIONAL RESULTS AND DISCUSSION

To test the computational efficiency and numerical stability of the developed mesoscopic model, we perform a series of simulations for a number of systems containing hundreds of interacting CNTs. Analysis the total energy conservation during the long-term evolution of the system is used to verify the correct implementation of the model, whereas the extent of the structural changes observed in the simulations is serving as an illustration of the capabilities of the model to study the mesoscopic structural rearrangements in the system.

All simulations are performed for samples composed of (10,10) nanotubes ( $R_T = 6.785 \text{ \AA}$ ). The interactions among CNTs are described by the tubular potential parameterized for interatomic potential given by Eq. (9). The initial tests simulations are performed for a relatively small sample containing 537 CNTs (Figs. 3, 5-7). Each CNT has a length of 180  $\text{\AA}$  and is represented by 9 segments. The initial sample has dimensions of  $600 \times 600 \times 600 \text{ \AA}^3$ , with periodic boundary conditions applied in all directions. The density of the sample is  $\approx 0.145 \text{ g/cm}^3$ .

The initial configuration of CNTs is generated with an algorithm in which the nanotubes are grown from random points inside the computational cell in a ‘segment-by-segment’ manner. Positions of new segments attached to the ones already present in the sample are chosen with the help of a stochastic ‘trial-and-error’ method aimed at minimizing the total energy of the sample. This method produces three-dimensional structure of randomly oriented slightly curved nanotubes (Fig. 3a) with relatively small inter-tube interaction energy.

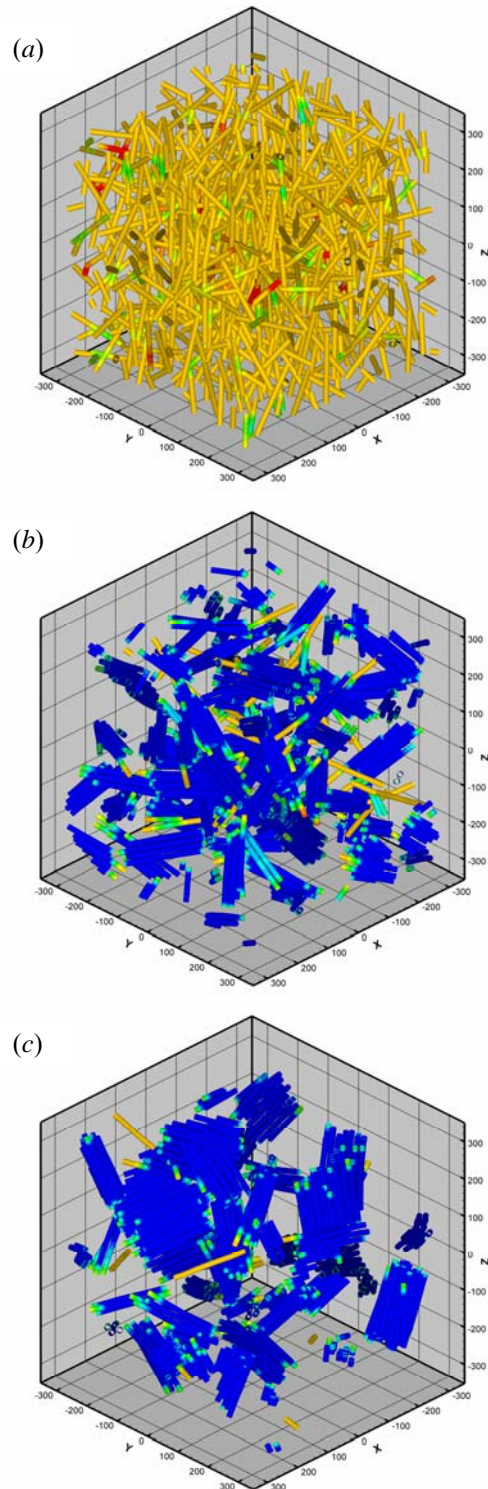


**Figure 3.** Snapshots from a simulation performed for a system of 537 (10,10) CNTs with the length of each CNT equal to 180 Å. The dimensions of the system are  $600 \times 600 \times 600 \text{ \AA}^3$  and the density is  $0.145 \text{ g/cm}^3$ . The snapshots are taken at times of 0 ns (a), 1 ns (b), and 4 ns (c) of the simulation. The CNTs are colored according to the local inter-tube interaction energy, with red corresponding to high and blue corresponding to low interaction energy.

The nanotube segments in Figs. 3 and 6 are colored according to the values of local inter-tube interaction energy, with yellow color corresponding to zero interaction energy. In the initial state, Fig. 3a, the interaction among CNTs is localized in a relatively small number of local regions colored red and green, with red segments having positive energy values corresponding to strong repulsion between CNTs. Thus, the initial structure of the computational samples consists of individual CNTs, which are not assembled into bundles.

Although the velocities of all nodes in the initial state are set to zero, the small initial inter-tube interaction is sufficient to trigger the evolution of the CNT configuration in a simulation illustrated by snapshots shown in Fig. 3. The snapshots from the simulation clearly show a spontaneous rearrangement of the initial random network of CNTs into well-defined bundles. Dark blue color of CNT segments in Fig. 3b,c corresponds to low values of inter-tube interaction energy characteristic of parallel tubes located close to the equilibrium distance from each other.

In the simulation illustrated in Fig. 3, the bundles of CNTs are formed on the time scale of hundreds of picoseconds, with almost all tubes grouped into bundles by 500 ps. Further evolution of the structure proceeds in the direction of gradual growth of the bundles. The final structure of the sample consists of several large bundles that have almost no interaction with each other. Obviously, this final structure is defined by the short length of the CNTs used in the simulation. Simulations of larger samples with more realistic length of CNTs (e.g. Fig. 4) predict the formation of a random network of CNT bundles with entangled CNT structures and complex inter-connections among the bundles. Qualitatively, the network of bundles in Fig. 4 is similar to experimental pictures of the surface of bucky paper or CNT films [4,5,6,7,8,9]. Quantitative comparison between the simulation results and experimental data, however, is hampered by the lack of reliable structural characteristics capable of providing quantitative description of CNT networks. Despite the recent efforts and some progress in the direction of designing methods for structural characterization of CNT structures [10,11,30], this important problem has not been resolved yet.

Theoretically, a perfect crystalline bundle of CNTs should exhibit hexagonal packing of nanotubes. The hexagonal arrangement of CNTs in the bundles has also been confirmed by experimental observations [4,6]. In simulations, the packing of nanotubes in bundles just after their formation is rather irregular. The long-term rearrangements of CNTs in the bundles, however, result in a gradual increase of the ordering of nanotubes, with local hexagonal arrangements appearing in the cross-sections of the bundles, e.g. Fig. 5. The number of nanotubes involved in the hexagonal structures increases with time, but the rate of the structural relaxation varies widely depending on the relaxation conditions (e.g., constant-energy vs. constant-temperature simulations, etc.). Even in the simulation performed with unrealistically short tubes, Fig. 3, the process of the relaxation inside the bundles and the

formation of hexagonal packing of CNTs takes long time and is not finished within 10 ns of the simulation. Hence, the process of bundle formation includes two basic stages: 1) relatively fast arrangement of individual CNTs into bundles with irregular structures, and 2) much slower re-arrangement of CNTs within the bundles resulting in a more ordered internal structure of the bundles.

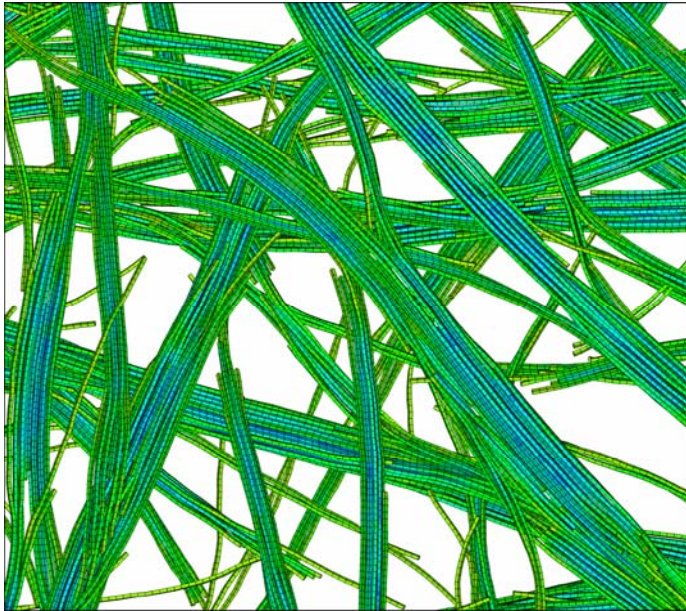


**Figure 4.** Random network of CNT bundles observed at 0.6 ns in a simulation performed for a sample consisting of 1543 (10,10) CNTs. The length of each CNT is equal to 200 nm, the dimensions of the system are  $500 \times 500 \times 20 \text{ nm}^3$ , and the density is  $0.2 \text{ g/cm}^3$ . Only a small part of the system is shown in the figure.

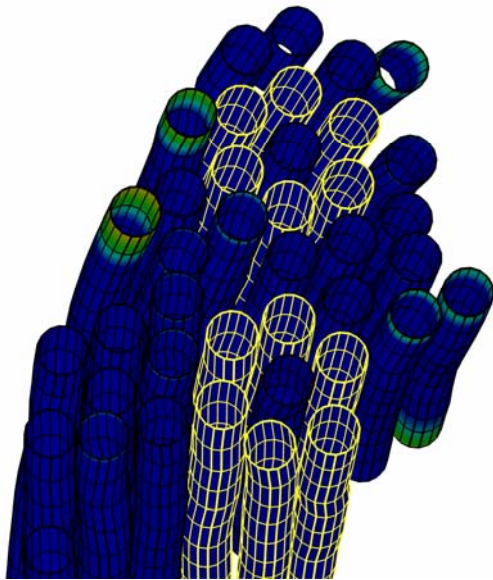


**Figure 5.** Enlarged view of a cross-section of a typical bundle from Fig. 3c. Representation of some of the CNTs is altered to highlight the

development of the hexagonal packing of CNTs in the bundle.

The applicability of the developed mesoscopic model for extreme conditions of high energy/material density is tested by applying high hydrostatic pressure to the sample shown in Fig. 3a. The pressure is applied using the Berendsen barostat, commonly used in MD simulations [29]. The barostat is modified for CNT-based materials so that only the size of the computational cell and the coordinates of the center of mass of CNTs are scaled in the algorithm, while the relative positions of nodes in the CNTs remain unaffected by the scaling. This procedure ensures that the scaling affects the inter-tube interaction forces, whereas much stiffer internal stretching and bending interactions remain unchanged. A test simulation illustrated in Fig. 6 demonstrates that the samples can be quickly compressed up to a density of  $0.6 \text{ g/cm}^3$  and even higher. The compressed state of the sample is characterized by strong repulsive interactions among the CNTs (red segments in Fig. 6b). At the same time, the nanotubes attain more curved shapes during the compression, resulting in the increase in the internal stretching and bending energies of the CNTs.

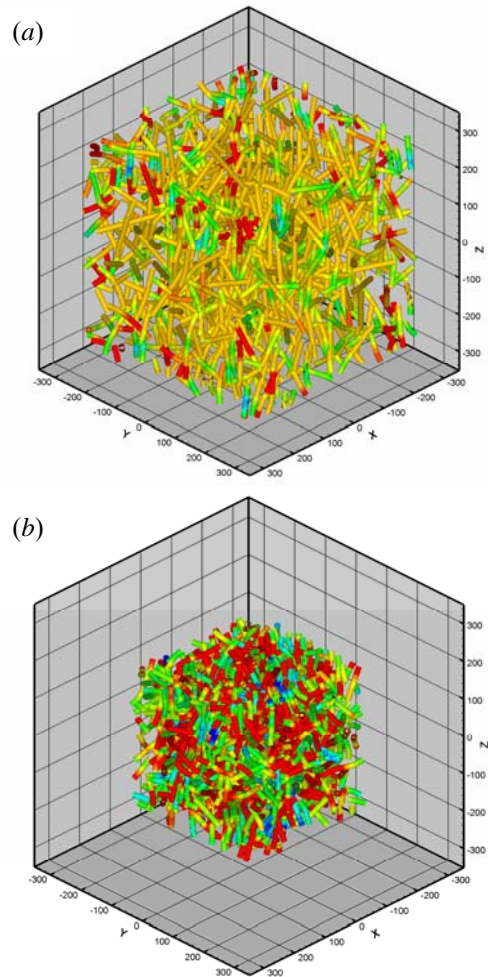


**Figure 6.** Snapshots of a system of CNTs shown in Fig. 3a after compression in the modified Berendsen barostat up to densities of 0.2

$\text{g/cm}^3$  (a) and  $0.6 \text{ g/cm}^3$  (b).

The total energy of the system,  $E+U$  as defined by Eqs. (3) and (4), is a quantity that must be conserved in a dynamic simulation based on the integration of the classical equations of motion, Eq. (2). The accuracy of the model, therefore, can be assessed by monitoring the quality of the total energy conservation during the simulations. With an appropriate choice of the timestep of integration of the equations of motion (on the order of 10 fs), the numerical drift in the total energy in the simulations is found to be relatively small even in long simulations performed for tens of nanoseconds. In particular, in the simulation discussed above and illustrated in Fig. 3, the accumulated drift in the total energy by the time of 8 ns is less than 2 % of the value of the inter-tube interaction energy  $|U_{\text{Int}}|$  at this time, Fig. 7. Equally good energy conservation is observed for much larger  $500 \times 500 \times 200 \text{ nm}^3$  systems containing  $\approx 15 \times 10^3$  nanotubes with the length of 200 nm each (total of  $1.5 \times 10^6$  dynamic nodes).

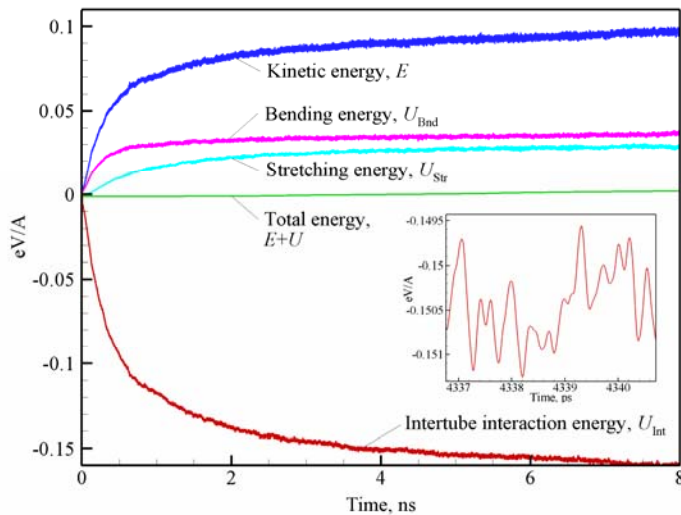


**Figure 7.** Evolution of the total energy  $E+U$  and its components  $E$ ,  $U_{\text{Str}}$ ,  $U_{\text{Bnd}}$ , and  $U_{\text{Int}}$  in a simulation illustrated in Fig. 3. The inset shows the variation of the inter-tube interaction energy  $U_{\text{Int}}$  on the time scale of picoseconds.

Analysis of multiple test simulations indicate that an acceptable level of the total energy conservation can not be achieved without the introduction of the weighted approach briefly described in Section 4.2. This approach ensures a smooth variation of the interaction energy  $U_{\text{IT}}$  during the relative motion of interacting nanotubes. All attempts to directly apply the tubular potential, Eq. (23), for the calculation of the segment-chain potential  $U_{\text{SC}}$  (e.g., by defining the ‘effective’ straight tube with the help of the closest segment-segment pair) resulted in a large drift in the total energy that becomes unacceptable at the time-scale of nanoseconds.

The requirements for achieving the accurate conservation of the total energy also include a careful numerical treatment of the tubular potential given by Eq. (23). The implementation of

this equation in the computational algorithm should account for conditions when  $\sin \alpha \rightarrow 0$ , resulting in the undefined form of the right part of Eq. (23), as well as for the presence of regions of very high gradients of  $\Phi(h, \zeta)$ . The computationally-efficient methods developed for dealing with these and other numerical problems are described elsewhere [28].

## SUMMARY

A novel tubular potential method for representation of the interaction between tubular dynamic elements is developed and implemented in a mesoscopic computational model for simulation of the collective behavior of CNTs in CNT-based materials. The method includes a computationally-efficient tubular potential for interaction between a segment and a straight tube, as well as a weighted approach for an accurate representation of the interactions among curved nanotubes. The tubular potential can be parameterized for an arbitrary law of interaction between surface elements representing atoms or molecules that build up the tubular structures and, therefore, can be adopted for simulation of systems consisting of various nano- and micro-tubular elements, such as nanotubes, nanorods, and micro-fibers.

First applications of the mesoscopic model enabled by the tubular potential demonstrate that the model exhibits good total energy conservation and is capable of simulating the structural evolution in CNT-based materials on a timescale extending up to tens of nanoseconds. The model predicts spontaneous self-assembly of CNTs into a continuous network of bundles with partial hexagonal ordering of CNTs in the bundles. The structures produced in the simulations are qualitatively similar to the structures of CNT films and bucky paper observed in experiments. The development of the model opens up possibilities to study the effective properties of CNT-based materials defined by the collective behavior of thousands of interacting nanotubes.

## ACKNOWLEDGMENTS

This work was supported by NASA through the Hypersonics project of the Fundamental Aeronautics program (NNX07AC41A), and by the National Science Foundation (NIRT-0403876).

## REFERENCES

- [1] Sinnott, S.B., and Andrews, R., 2001, “Carbon Nanotubes: Synthesis, Properties, and Applications,” *Critical Rev. Solid State and Mater. Sci.* **26**, pp. 145–249.
- [2] Srivastava, D., Wei, C., and Cho, K., 2003, “Nanomechanics of Carbon Nanotubes and Composites,” *Appl. Mech. Rev.* **56**, pp. 215–229.
- [3] Hu, Y.H., Shenderova, O.A., Hu, Z., Padgett, C.W., and Brenner, D.W., 2006, “Carbon Nanostructures for

- Advanced Composites,” *Rep. Prog. Phys.* **69**, pp. 1847–1895.
- [4] Thess, A., Lee, R., Nikolaev, P., Dai, H., Petit, P., Robert, J., Xu, Ch., Lee, Y.H., Kim, S.G., Rinzler, A.G., Colbert, D.T., Scuseria G.E., Tomanek, D., Fischer, J.E., and Smalley, R.E., 1996, “Crystalline Ropes of Metallic Carbon Nanotubes,” *Science* **273**, pp. 483–487.
- [5] Liu, J., Rinzler, G., Dai, H., Hafner, J.H., Bradley, R.K., Boul, P.J., Lu, A., Iverson, T., Shelimov, K., Huffman, C.B., Rodriguez-Macias, F.J., Shon, Y.-S., Lee, T.R., Colbert, D.T., and Smalley, R.E., 1998, “Fullerene Pipes,” *Science* **280**, pp. 1253–1256.
- [6] Rinzler, A.G., Liu, J., Dai, H., Nikolaev, P., Huffman, C.B., Rodriguez-Macias, F.J., Boul, P.J., Lu, A.H., Heymann, D., Colbert, D.T., Lee, R.S., Fischer, J.E., Rao, A.M., Eklund, P.C., and Smalley, R.E., 1998, “Large-Scale Purification of Single-Wall Carbon Nanotubes: Process, Product, and Characterization,” *Appl. Phys. A* **67**, pp. 29–37.
- [7] Sreekumar, T.V., Liu, T., Kumar, S., Ericson, L.M., Hauge, R.H., and Smalley, R.E., 2003, “Single-Wall Carbon Nanotube Films,” *Chem. Mater.* **15**, pp. 175–178.
- [8] Ma, W., Song, L., Yang, R., Zhang, T., Zhao, Y., Sun, L., Ren, Y., Liu, D., Liu, L., Shen, J., Zhang, Zh., Xiang, Y., Zhou, W., and Xie, S., 2007, “Directly Synthesized Strong, Highly Conducting, Transparent Single-Walled Carbon Nanotube Films,” *Nanoletters* **7**, pp. 2307–2311.
- [9] Poulin, P., Vigolo, B., and Launois, P., 2002, “Films and Fibers of Oriented Single Wall Nanotubes,” *Carbon* **40**, pp. 1741–1749.
- [10] Berhan, L., Yi, Y.B., and Sastry, A.M., 2004, “Effect of Nanorope Waviness on the Effective Moduli of Nanotube Sheets,” *J. Appl. Phys.* **95**, pp. 5027–5034.
- [11] Berhan, L., Yi, Y.B., Sastry, A.M., Munoz, E., Selvidge, M., and Baughman, R., 2004, “Mechanical Properties of Nanotube Sheets: Alteration in Joint Morphology and Achievable Moduli in Manufactured Material,” *J. Appl. Phys.* **95**, pp. 4335–4345.
- [12] Harik, V.M., 2002, “Mechanics of Carbon Nanotubes: Applicability of the Continuum-Beam Models,” *Comp. Mat. Sci.* **24**, pp. 328–342.
- [13] Das, P.S., and Wille, L.T., 2002, “Atomistic and Continuum Studies of Carbon Nanotubes under Pressure,” *Comp. Mat. Sci.* **24**, pp. 159–162.
- [14] Arroyo, M., and Belytschko, T., 2004, “Finite Element Methods for the Non-linear Mechanics of Crystalline Sheets and Nanotubes,” *Int. J. Numer. Methods Eng.* **59**, pp. 419–456.
- [15] Gou, J., and Lau, K.-T., 2006, “Modeling and Simulation of Carbon Nanotube/Polymer Composites”, in *Handbook of Theoretical and Computational Nanotechnology*, ed. Rieth, M., and Schommers, W., American Scientific Publishers, Stevenson Ranch, chapter 66.
- [16] Colbourn, E.A. (editor), 1994, *Computer Simulation of Polymers*, Longman Scientific and Technical, Harlow.
- [17] Buehler, M.J., 2006, “Mesoscale Modeling of Mechanics of Carbon Nanotubes: Self-assembly, Self-folding, and Fracture,” *J. Mater. Res.* **21**, pp. 2855–2869.
- [18] Zhigilei, L.V., Wei, C., and Srivastava, D., 2005, “Mesoscopic Model for Dynamic Simulations of Carbon Nanotubes,” *Phys. Rev. B* **71**, 165417.
- [19] Dresselhaus, M.S., Dresselhaus, G., and Saito, R., 1995, “Physics of Carbon Nanotubes,” *Carbon* **33**, pp. 883–891.
- [20] Islam, M.F., Rohas E., Bergey, D.M., Johnson, A.T., and Yodh, A.G., 2003, “High Weight Fraction Surfactant Solubilization of Single-Wall Carbon Nanotubes in Water,” *Nanoletters* **3**, pp. 269–273.
- [21] Landau L.D., and Lifshitz, E.M., 1976, *Mechanics*, 3rd ed., Butterworth-Heinemann, Oxford.
- [22] Stuart, S.J., Tutein, A.B., and Harrison, J.A., 2000, “A Reactive Potential for Hydrocarbons with Intermolecular Interactions,” *J. Chem. Phys.* **112**, pp. 6472–6486.
- [23] Girifalco, L.A., Hodak, M., and Lee, R.S., 2000, “Carbon Nanotubes, Buckyballs, Ropes and a Universal Graphitic Potential,” *Phys. Rev. B* **62**, pp. 13104–13110.
- [24] The cutoff of the non-bonding interaction potential at large distances is not explicitly discussed in Ref. [22] but is used in the code implementing AIREBO potential and provided to us by Steven Stuart of Clemson University. The values of  $r_c$  and  $r_{c0}$  listed in Table 1 are from the code.
- [25] Stan, G., Bojan, M.J., Curtarolo, S., Gatica, S.M., and Cole, M.W., 2000, “Uptake of Gases in Bundles of Carbon Nanotubes,” *Phys. Rev. B* **62**, pp. 2173–2180.
- [26] Sun, C.-H., Yin, L.-C., Li, F., Lu, G.-Q., and Cheng, H.-M., 2005, “Van der Waals Interactions between Two Parallel Infinitely Long Single-Walled Nanotubes,” *Chem. Phys. Lett.* **403**, pp. 343–346.
- [27] Jiang, L.Y., Huang, Y., Jiang, H., Ravichandran, G., Gao, H., Hwang, K.C., and Liu, B., 2006, “A Cohesive Law for Carbon Nanotube/Polymer Interfaces Based on the van der Waals Force,” *J. Mech. and Phys. Solids* **54**, pp. 2436–2452.
- [28] Volkov, A.N., and Zhigilei, L.V., “Tubular Potential for Simulation of Systems Composed of Nanotubes or Other Nano-/Micro-tubular Structural Elements,” in preparation.
- [29] Allen, M.P., and Tildesley, D.J., 1987, *Computer simulation of liquids*, Clarendon Press, Oxford.
- [30] Yi, Y.B., Berhan, L., and Sastry, A.M., 2004, “Statistical Geometry of Random Fibrous Networks, Revisited: Waviness, Dimensionality, and Percolation,” *J. Appl. Phys.* **96**, pp. 1318–1327.